J Nanostruct 15(1): 344-357, Winter 2025

RESEARCH PAPER

Deposition of Graphene Nanoparticles Prepared by Laser Ablation Method Mixed with Chlorophyll Dye on Silicon Nanowire Substrate as a Detector

Elaf Ayad Khadim*, Mohammed Hamza. K. AL-Mamoori, Saif Mohammed Hassan

Department of physics, College of Science for Women, University of Babylon, Hilla, Iraq

ARTICLE INFO

Article History:
Received 07 September 2024
Accepted 28 December 2024
Published 01 January 2025

Keywords:
Graphene nanoparticles
Silicon nanowire
Chlorophyll dye
Nanocomposite

ABSTRACT

Numerous fields find semiconductor nanowires, especially silicon nanowires (SiNWs), appealing due to their distinct electronic characteristic. Accordingly, in this research, A GNPs/Chl./SiNWs nanocomposite was fabricated using laser pulses with a fundamental wavelength of 1064 nm and an energy of 200 mJ/pulse, all at a repetition rate of 5 Hz and 200 pulses. The properties of this nanocomposite were studied through scanning electron microscope (SEM), X-ray diffraction (XRD) and FTIR, as well as the optical properties were studied through UV-Vis. Diffused reflectance spectroscopy and Raman spectra of GNPs/Chl./SiNWs nanocomposite. The results show the XRD of GNPs/Chl./SiNWs nanocomposite at pH=3, has cubic silicon structure with the formation of graphene and graphene oxide nanoparticles. Silicon nanowire was prepared by chemical etching (EMACE) technique with a diameter of 137 nm and a length of 400 nm. GNPs/Chl./SiNWs nanocomposite show the graphene is formed in the form of spherical particles with the mean of dimeter of silicon nanowires is about 135.7 nm. FTIR results showed the formation of graphene and graphene oxide. The results reveal that modifying the surface morphology of the Si substrate to form SiNW successfully reduced the reflection loss of incident radiation over a broad spectral range. Also, GNPs/Chl./SiNWs nanocomposite was used in manufacturing a photodetector and all its parameters were calculated with a quantitative efficiency of up to to18.9% at 650 nm.

How to cite this article
Khadim E., AL-Mamoori M., Hassan S. Deposition of Graphene Nanoparticles Prepared by Laser Ablation Method Mixed with Chlorophyll Dye on Silicon Nanowire Substrate as a Detector . J Nanostruct, 2025; 15(1):344-357. DOI: 10.22052/JNS.2025.01.033

INTRODUCTION

Silicon-based materials have garnered considerable interest because of their unique properties and potential applications in broad areas, including electronics [1–6], thermoelectric [7], solar energy harvesting [8–11], and biotechnology [12, 13]. With a room temperature band gap of 1.12 eV, silicon promises efficient solar energy harvesting across the entire solar spectrum from ultraviolet (UV) to near infrared (IR). For photodetector, nanostructured materials typically exhibit much better activity than their bulk counterparts because of their large surface areas and short charge carrier diffusion distances [10, 14–17].

Graphene, a single atomic layer of a honeycomb lattice of carbon atoms, has recently become the central focus of material research for fundamental studies because of its potential applications in diverse areas [18–25]. The covalently bonded

* *Corresponding Author Email: Elaf.ayad1991@gmail.com*

carbon lattice can exhibit excellent chemical stability and function as a natural protective barrier. For example, it has been shown that graphene can function as an effective passivation layer to protect metal surfaces from oxidation [26, 27]. Additionally, graphene can exhibit excellent electrical transport properties and facilitate charge separation and transport in semiconductors and their interfaces [28–30]. Lastly, single or few-layer graphene sheets exhibit high optical transparency at visible wavelengths [31], which will not affect the light absorption of underlying materials. Together, these combined attributes make graphene an excellent candidate as a novel protection material and charge- mediating layer for SiNW photocatalysts.

On the other hand, chlorophyll is a cheap and easily extractable most abundant bio-molecule in the photosynthetic system of green plants, bryophytes, algae, and bacteria [32–34]. Chl.

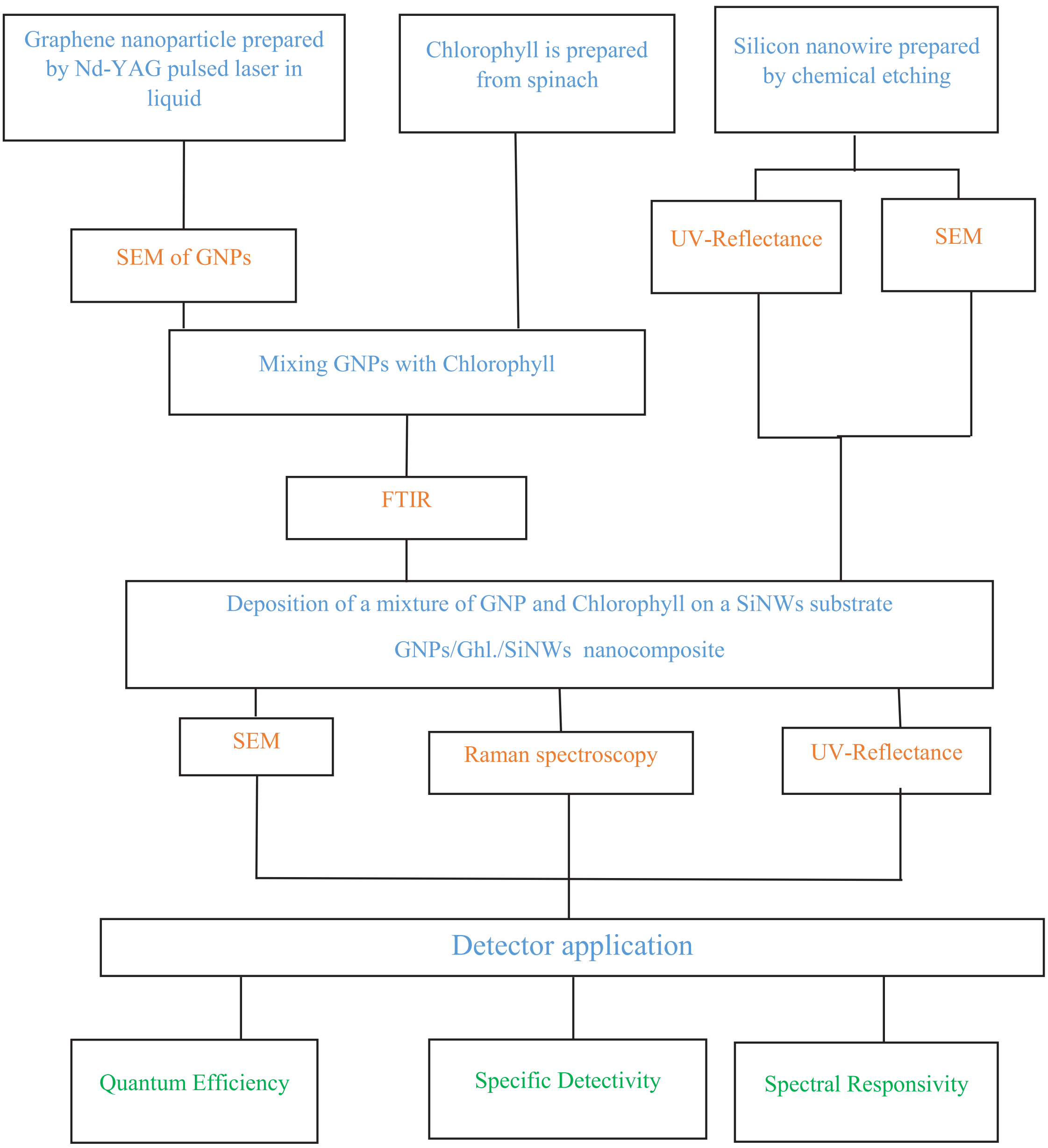

Fig. 1. Flow chart showing the steps for preparing and measurements of GNPs/Ghl./SiNWs nanocomposite.

possesses two strong absorption bands, one is Soret-band in the range of 410 nm-450 nm and other is Q-band in the range of 600 nm-700 nm [32,34,35]. The spectral characteristics of Chl. are explained by Gouterman four orbital model [36,37], which are HOMO-1 (highest occupied molecular orbital), HOMO, LUMO (lowest unoccupied molecular orbital) and LUMO+1. Not only light absorption, Chl. also plays a crucial role in the transfer of absorbed photon energy in terms of excitons through resonance energy transfer to the reaction centers of photosystems [33–35]. Chl. contains porphyrin ring with a central magnesium (Mg) atom surrounded by four nitrogen atoms, which is mainly responsible for light-harvesting and energy transfer [33,34]. Efforts have already been made to utilize this excellent property of Chl. in different kinds of devices such as dye-sensitized solar cells [32,38-40], photo detector [41,42] and photoelectrode [43–46]. But the reported efficiencies are not up to the mark due to the absence of proper photo-excited charge transfer system, which can be escalated with the introduction of suitable material like graphene [32,41].

MATERIALS AND METHODS

General Consideration

A JSM-6510LV scanning electron microscopy (FESEM) measured the morphology of the samples (Type - S-1640 HITACHI company Japan). The sample structure was analyzed using (Cu Kα) radiation (λ=1.5406 Å) in reflection geometry with a Shimadzu 6000 X-ray diffractometer (made in JAPAN). For some pure samples and all doped samples, Mid-IR spectra, from (4000 - 400 cm^{-1}), were obtained using FTIR-Spectrometer, supplied by ALPHA (Made in Germany). KBr powder was mixed with powder samples in order to determination of the spectra for FTIR. A UV-Vis diffused reflectance spectroscope was used to obtain the optical properties (CECIL CE 7200, ENGLAND) of all prepared materials.

Preparation of Graphene/chlorophyll/silicon nanowires (GNPs/Chl./SiNWs) nanocomposite

In the first stage, Graphene nanoparticles (GNPs) were produced by Q-Switched Nd: YAG pulsed laser in liquids (PLAL-Method). after placing the graphite pellet in a clean beaker and submerging it in 5 mL of deionized water, it is removed using laser pulses with a fundamental wavelength of 1064 nm and an energy of 200 mJ/pulse, all at a repetition rate of 5 Hz and 200 pulses. As shown in the Fig. 1.

In the second stage, the chlorophyll (Chl.) was prepared from spinach as shown in the Fig. 1, the and Chlorophyll Extraction was prepared as Ten milliliters of 80% acetone were used to grind five grams of freshly chopped leaves. Then, for five minutes, it was centrifuged at 5000–10000 rpm. Once the supernatant was moved, the process was repeated until the residue lost all of its color [47].

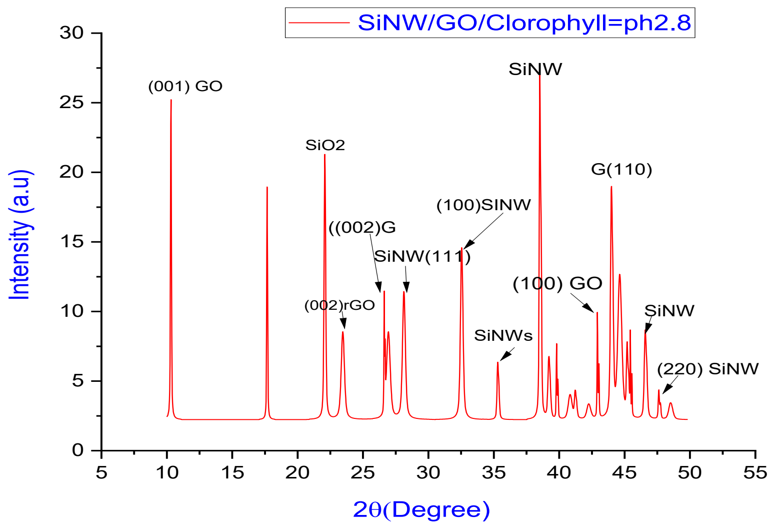

Fig. 2. Illustrated the XRD of GO/ Chlorophyll/ SiNWs nanocomposite.

In the third stage, silicon nanowire (SiNWs) was prepared as shown in the Fig. 1 as follows: The Si (p type) wafer was cleaned with acetone and isopropyl alcohol, and dried by using air gun. Si wafer (p type) were initially ultrasonically degreased in acetone and ethanol for 10 minutes, respectively. After each cleaning step, the Si pieces were thoroughly rinsed with DI water. The cleaned Si pieces were coated with Ag nanoparticle film by electroless metal deposition method in aqueous solution of 5% HF and 0.02 M $AgNO_3$ for 1 minute, and then immediately introduced in the electrochemical cell that exposing 1.0 cm 2 of the surface to the aerated 10% HF aqueous

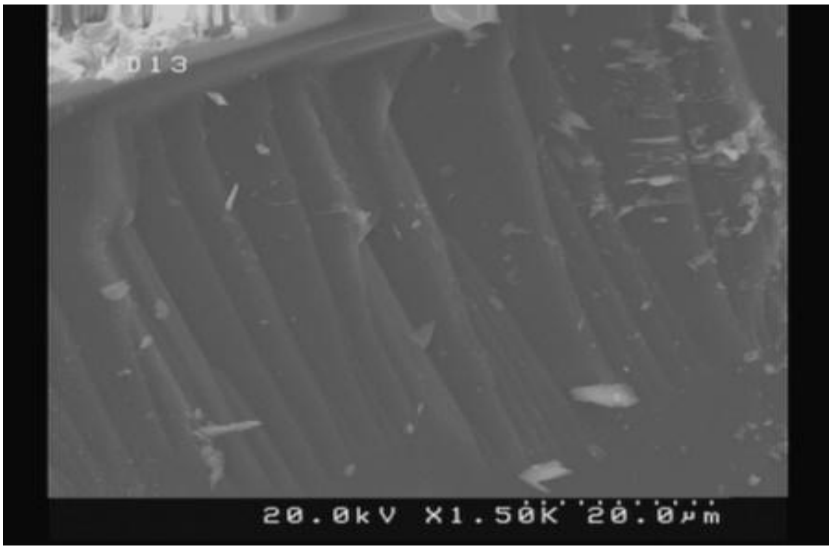

Fig. 3. SEM of silicon nanowires obtained by the chemical etching (EMACE) technique [62].

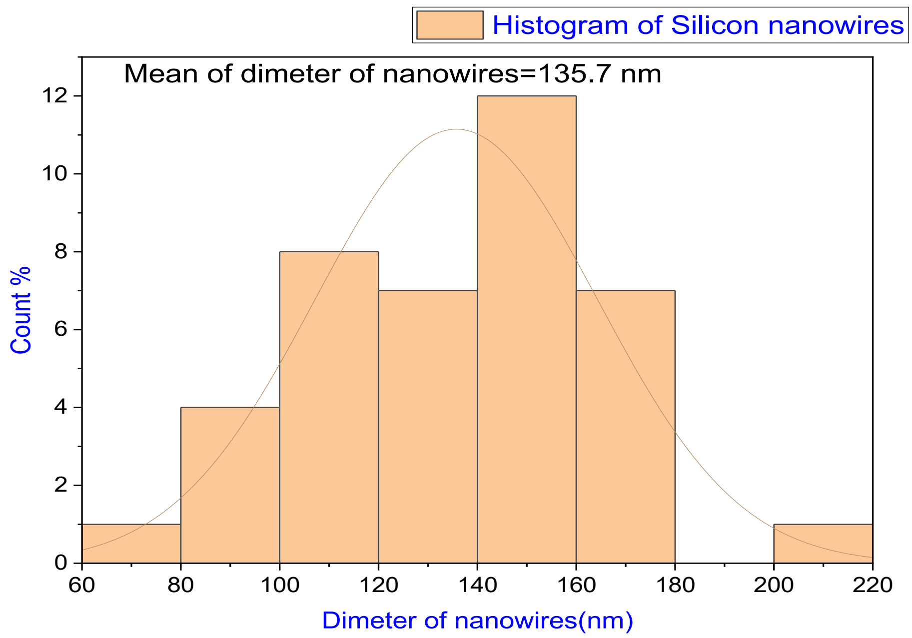

Fig. 4. The histogram of silicon nanowires.

solution. Silver glue was used on the back side of the Si substrate in contact with the copper plate to establish an ohmic contact. Subsequently, Si substrate is electrically connected to graphite

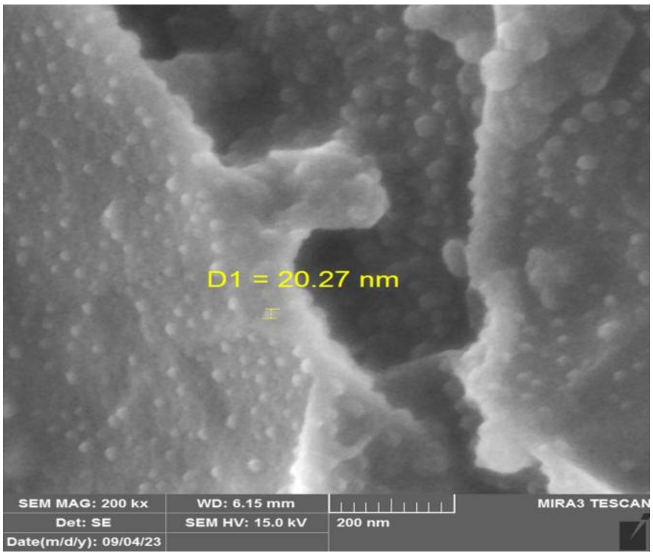

Fig. 5. FESEM images of GNPs.

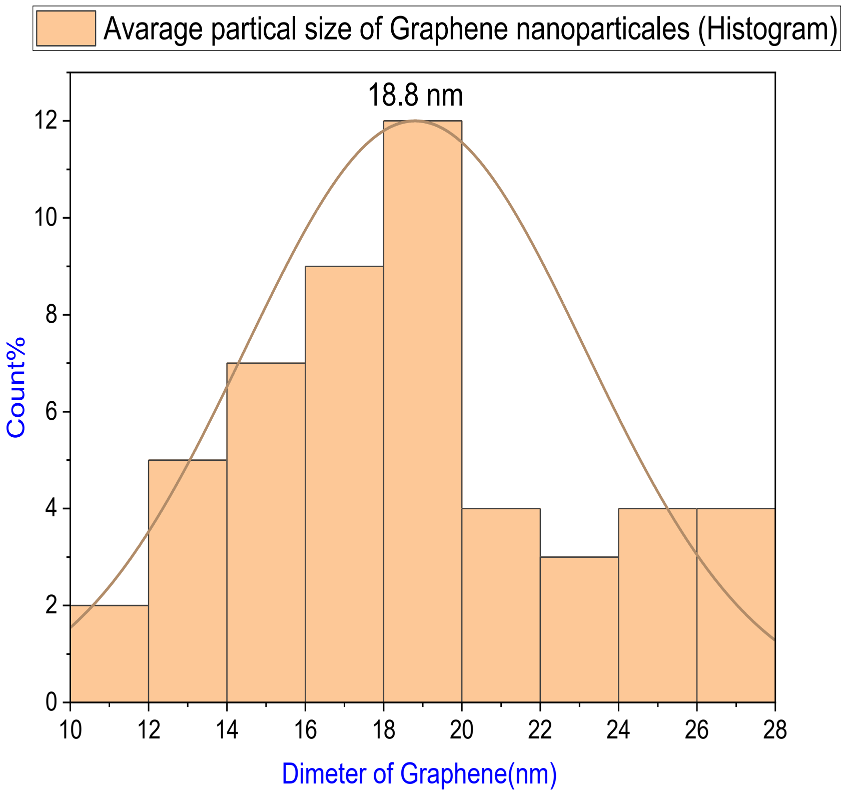

Fig. 6. The average particles size of GNPs.

rod through an external copper wire. he first peak corresponds to the silicon nanowires, while the latter two peaks are attributed to graphene. Notably, shifts in peak positions suggest effects related to the size distribution of the nanowires. This study underscores the interactions between silicon nanowires and graphene, enhancing our understanding of their combined properties in nanocomposite applications.

RESULTS AND DISCUSSION

X-ray Diffraction Analysis

Fig. 2 illustrated the XRD of GNPs/Chl./SiNWs nanocomposite at pH=3, the main peaks locate

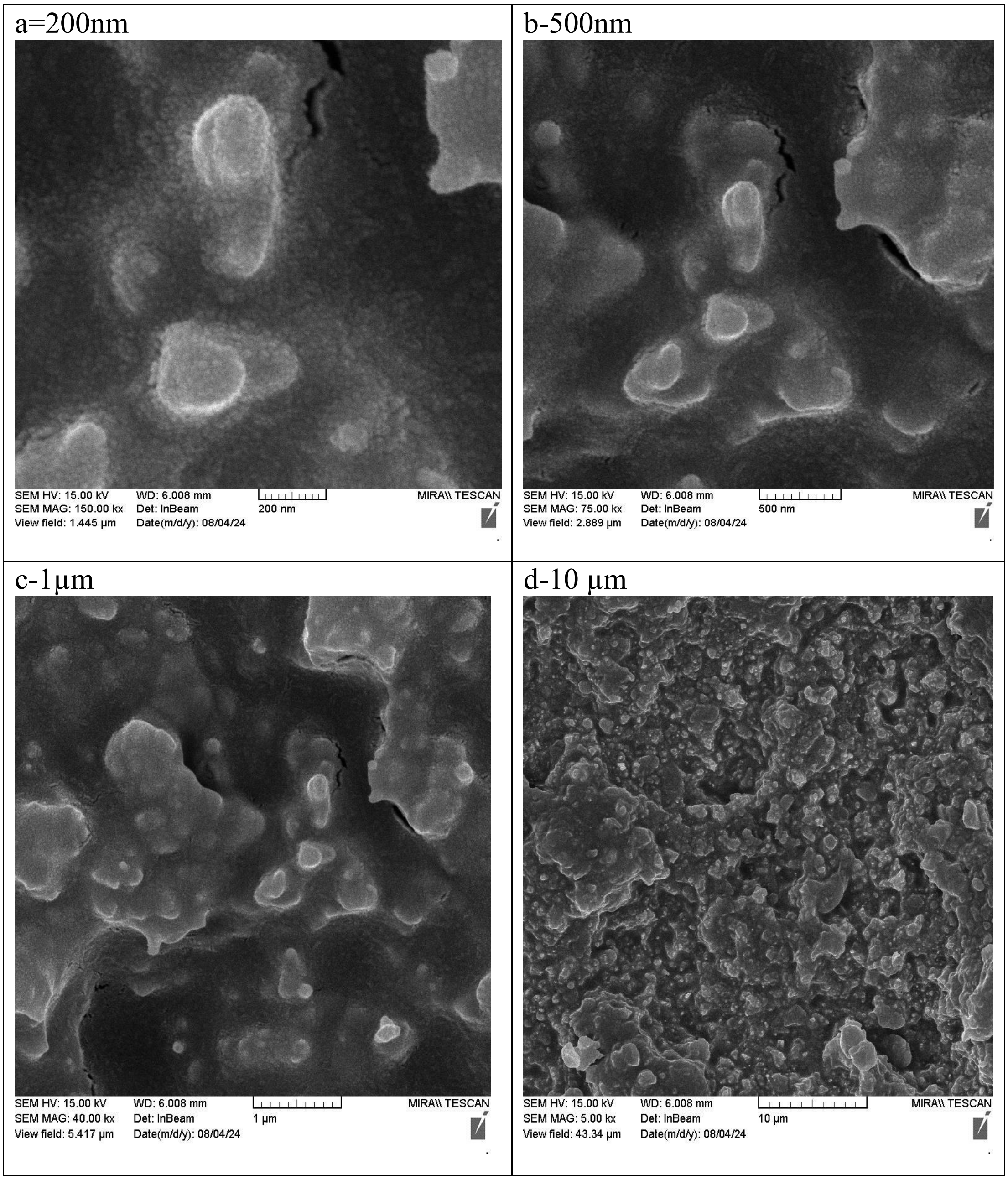

Fig. 7. The FESEM of GNPs/ Chlorophyll/ / SiNWs nanocomposite, a-200nm b-500nm c- 1µm d-10 1µm.

at 28.2°, 32.6°, 35.2, 38.5°, 39.3° and 48.5° corresponding to (111), (100), (100) (110) and (220) planes of cubic silicon structure and it is identical to what the researcher mentioned in the references [48,49,50]. but the peaks locate at 10.4°, 26.6° and 42.9 corresponding to (001), (002) and (100) planes of graphene oxide and graphene [51,52]. A diffraction angle of 22.1° was observed, possibly due to the presence of SiO_2.

Morphological investigations of nanocomposite

When a silicon surface is nanostructured, low reflection and strong absorption of visible light can be obtained. Such a silicon is called a black silicon and can be made by different techniques leading to different surface structures. By using the chemical etching (EMACE) technique [53], a very thin nanowire can be obtained Fig. 3. This kind of structure is very interesting for making detectors because electrons are conducted in the axis of the wires, while photons are well absorbed for a large range of incident angles.

The mean of dimeter of silicon nanowires is about 135.7 nm was also calculated using the image J program as shown in the Fig. 4.

Fig. 5 shows FESEM images of graphene nanoparticles (GNPs), it is clear that the graphene is formed in the form of spherical particles and in different sizes and homogeneously distributed, as is clear from the FESEM images in Fig. 4. The mean of dimeter of graphene nanoparticles is about 18.8 nm was also calculated using the image J program as shown in the Fig. 6.

Fig. 7 shows FESEM images of GNPs/Chl./SiNWs nanocomposite, it is clear that also, the graphene is formed in the form of spherical particles in different sizes and concentrated in small and large groups. The mean of dimeter of GNPs/Chl./SiNWs nanocomposite is about 23.6 nm as shown in the Fig. 8.

Fourier Transform Infrared (FTIR) Analysis

Fig. 9 show the spectrum of GNPs/Chl. nanocomposite shows prominent peaks at 3399 cm^{-1}, which corresponds to O–H stretching vibrations of carboxylic acids [54]. Characteristic absorption peaks appearing at 1694, 1369 and 1230 cm^{-1} in the FTIR spectra showed the presence of carboxyl C=C, alkoxy C–O stretching vibrations, and epoxy C–O, respectively [54,55,56,57].

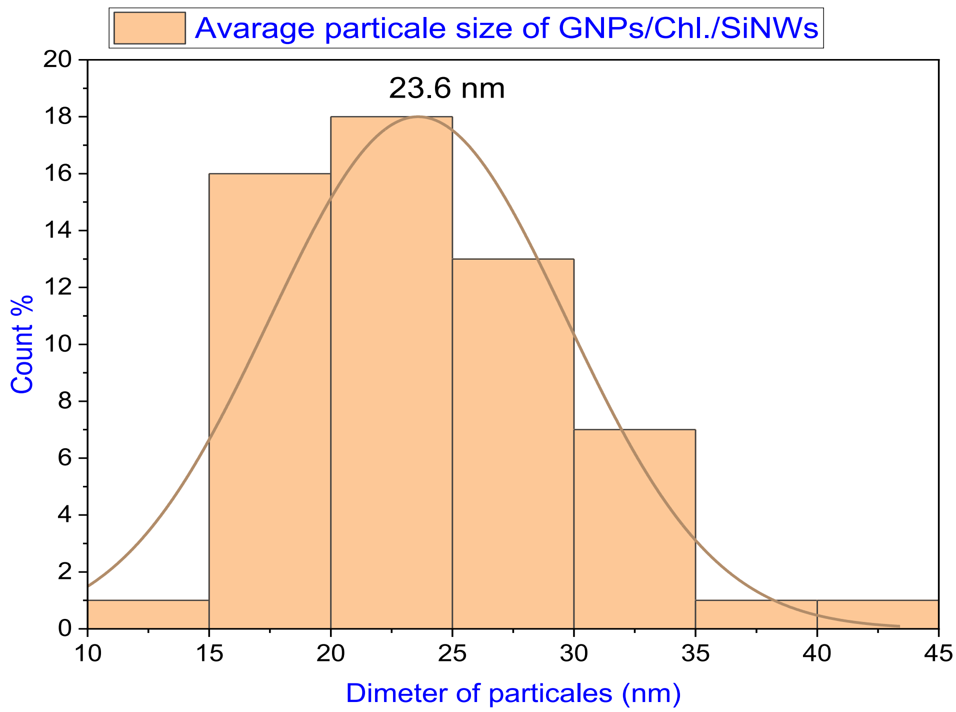

Fig. 8. The average particles size of GNPs/Chl./SiNWs Nanocomposite at PH=3.

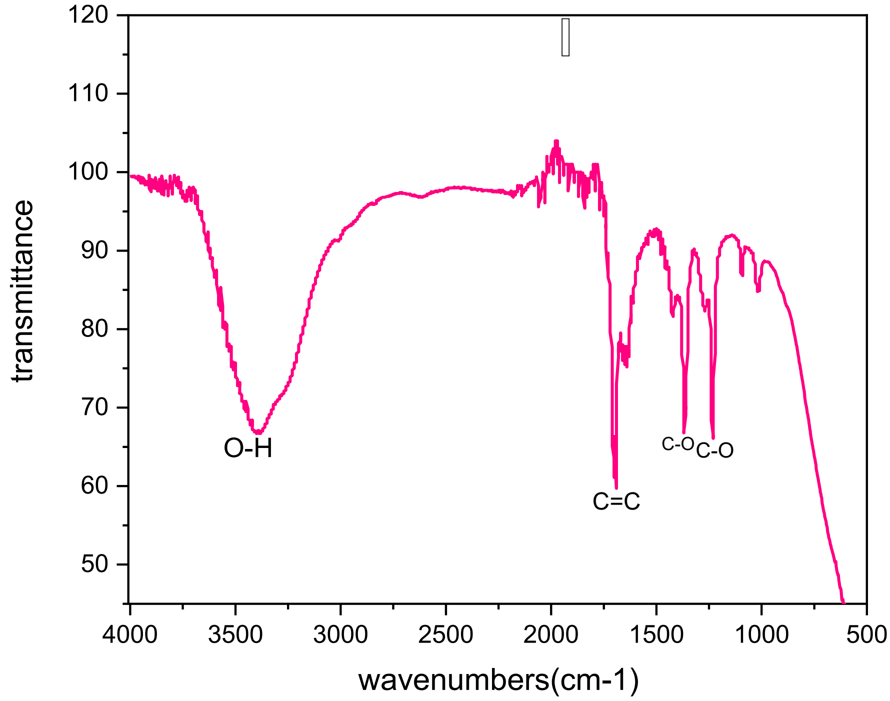

Fig. 9. FTIR spectra of GNPs /Chl. Nanocomposite.

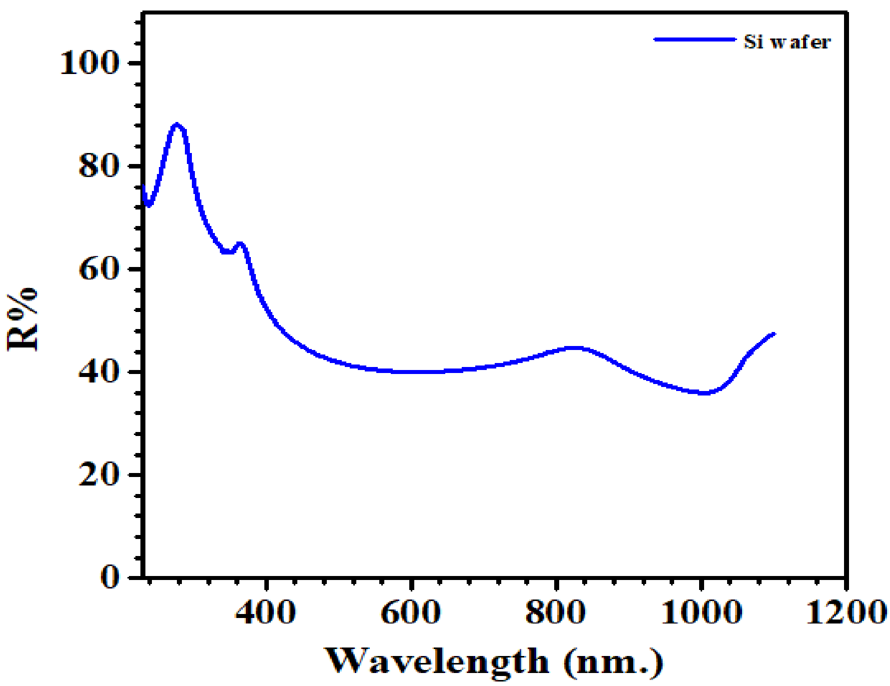

Fig. 10. The reflectance spectrum of Silicon wafer [58].

UV-Diffused Reflectance Spectroscopy

The fabrication of SiNWs is a surface modification technique that aims to minimize the reflection of incident light and increase the absorption as much as possible. The antireflective nature of the SiNWs has drawn attention since one of the major energy loss mechanisms of solar cells is optical reflection; the utilization of these nanostructures in photosensitive devices may eliminate the need for antireflective coatings. Fig. 10 shows the variation in reflectance (R) depending on the wavelength (λ) of incident radiation on the Si substrate [58]. The measurement was obtained by illuminating samples with radiation varying from the ultraviolet region (UV) to the infrared region (IR) with wavelengths ranging from 200 to 1100 nm. The reflectivity of Si wafers is quite high, exceeding 88% (maximum) and 65% (minimum) in the ultraviolet (UV) regions and decreasing in the IR region to 48% [58]. That is, there is no peak or absorption edge in the reflectivity spectrum of a silicon wafer in the visible region of the electromagnetic spectrum.

Fig. 11 was showed the reflectance of GNPs/Chl./SiNWs nanocomposite is much lower than that of their bare Si wafer counterpart and it is similar to what is stated in the reference [58]. It is clear that there is a slope between 400-700 nm, and this behavior is different from silicon wafer (i.e., the longer the wavelength, the lower the reflectivity and the higher the absorbance) due to the effect of graphene and chlorophyll deposited on the silicon nanowire. This simply indicates that the sample is very sensitive to visible compared to silicon wafer. This wavelength range (400 -700 nm) is essential for photosensitive device applications. The maximum and minimum reflectance of the sample is approximately 59% and 54% respectively in the UV range while the maximum and minimum reflectance of the sample is approximately 52% and 31% respectively in the visible range (400-700) nm. The results reveal that modifying the surface morphology of the Si substrate to form SiNW successfully reduced the reflection loss of incident radiation over a broad spectral range. This remarkable property suggests that SiNW arrays are a good candidate for antireflective surfaces and absorption materials in photovoltaic cell [58].

Raman spectroscopy

The common properties of graphene in Raman spectroscopy are known to be in the

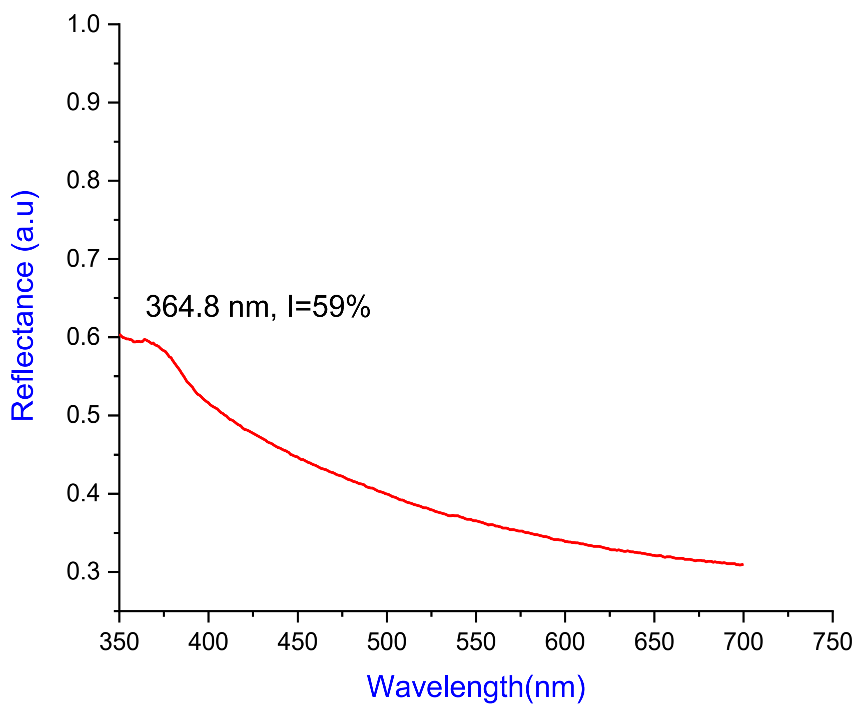

Fig. 11. The reflectance spectrum of GNPs/Chl./SiNWs nanocomposite.

wavelength range of (800–3000) cm^{-1}, which is in accordance with the electronic characteristics of graphite materials. Three prominent peaks, referred to as the G, D, and 2D bands, are located at approximately (1580, 1350, and 2700) cm^{-1} [59–61]. At the middle of the Brillouin zone,

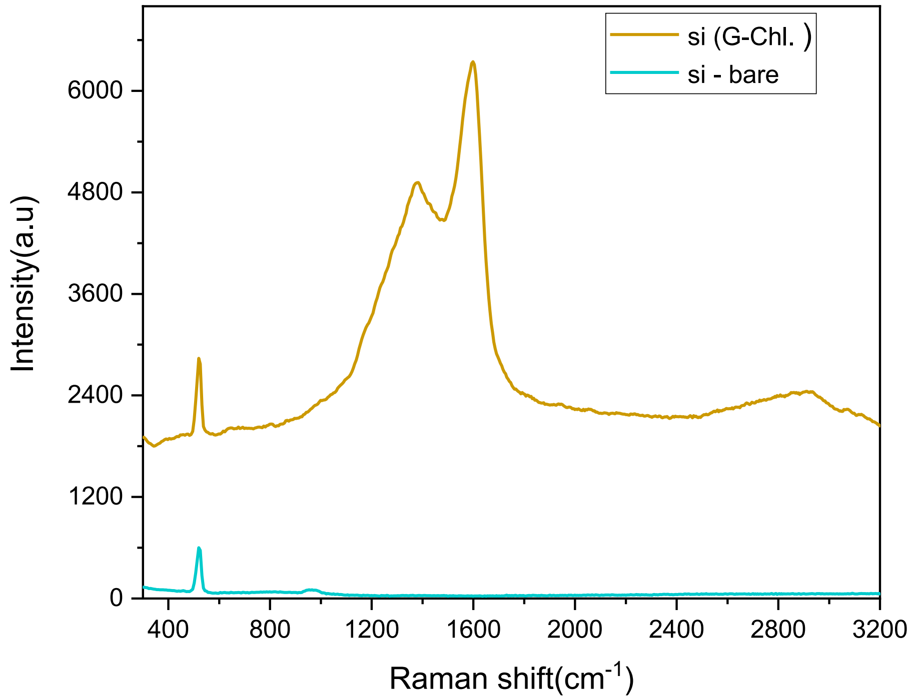

Fig. 12. The Raman spectrum of GNPs/Chl./SiNWs nanocomposite.

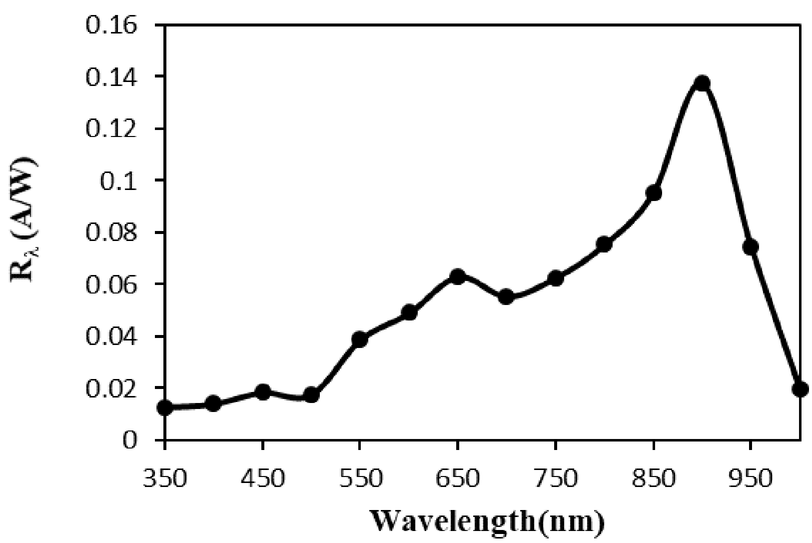

Fig. 13. The spectral responsivity as a function of wavelength.

the G band associates with the E_{2g} phonon [58]. Another fingerprint peak in graphite material with a concentration of faults is the disorder-induced D band [60]. The double resonant Raman scattering with two-phonon emissions is the source of a 2D peak, which is the second order of the D peak [59,61] as shown in Fig. 12.

For silicon nanowires, various recent papers reported Raman spectra of SiNWs. They report peak positions of 500-510 cm^{-1} for wires 10-15 nm in diameter [62-72].

It is noted through the Raman spectrum Fig. 12 that the silicon bare peak appears at (520cm^{-1}),but in the nanocomposite, three peaks appeared with a higher intensity at (520,1382,1598)cm^{-1} respectively. Where the first peak belongs to the

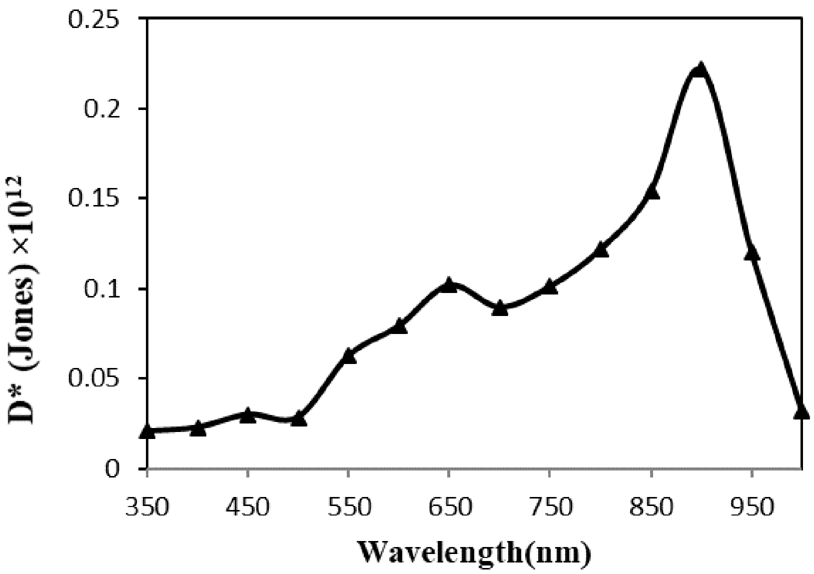

Fig. 14. The specific detectivity as a function of wavelength.

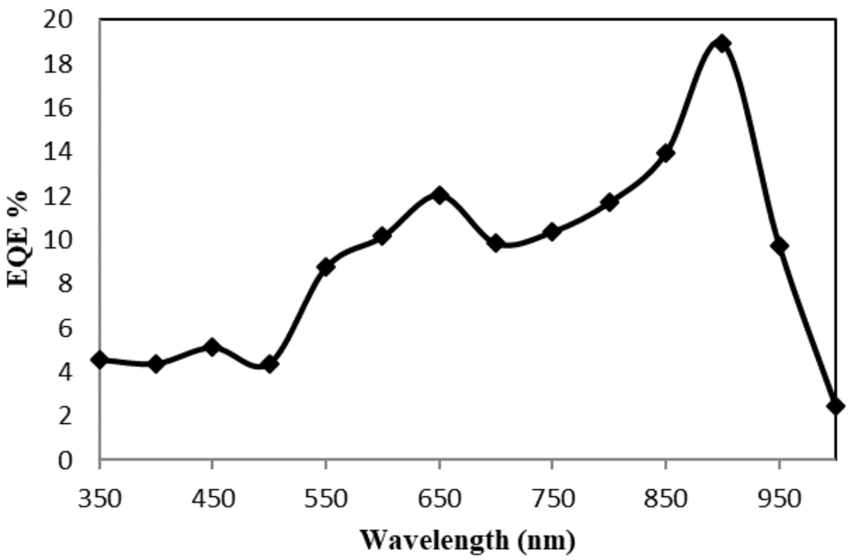

Fig. 15. The quantum efficiency as a function of wavelength.

silicon nanowire and the other two peaks belong to graphene. There is a shift in the peaks which is a result of the size distribution of the nanowires, some of which may be of small diameters.

Photodetector Parameters Measurement

The Spectral Responsivity (R_λ)

The spectral responsivity of structures in the (350-1000) nm wavelength region at a (3)V bias voltage was calculated using Eq. 1.

$$R_\lambda = \frac{I_{photocurrent}}{P_{input}} \text{ (A/W) or } \frac{V_{photovoltge}}{P_{input}} \text{ (V/W)} \quad (1)$$

The spectral responsivity graphs of the Ag/PSi/GNPs/Chl./Ag structure constructed are displayed as a function of wavelength in Fig. 13. According to the Fig. 13, the Ag/PSi/GNPs/Chl./Ag spectral responsivity curve has many response peaks, with the absorption edge of silicon responsible for the maximum peak at (900) nm, which is consistent with earlier research [73].

Specific Detectivity (D)*

The performance of the detector is correlated with specific detectivity, an essential parameter for a photodetector that indicates the lowest detectable power. The specific detectivity was calculated using Eq. 2.

$$D^* = R_\lambda \frac{\sqrt{A.\Delta f}}{I_n} \ (\text{cm.Hz})^{1/2}.\text{W}^{-1} \quad (2)$$

The specific detectivity for Ag/PSi/GNPs/Chl./Ag photodetectors is plotted against wavelength in Fig. 14. This graph demonstrate the direct relationship between particular detectivity and responsivity. It was discovered that the specific detectivity was (1.01×10^{12}) cm.$Hz^{1/2}W^{-1}$ for Ag/PSi/GNPs/Chl./Ag photodetector at wavelength (650) nm.

Quantum Efficiency

The quantum efficiency was calculated using Eq. 3.

$$\eta_{quantum} = \frac{R \times 1.24}{\lambda_{(\mu m)}} \times 100\% \quad (3)$$

The quantum efficiency of the Ag/PSi/GNPs/Chl./Ag structure as a function of wavelength (350–1000) nm is displayed in Fig. 15. The highest peak quantum efficiency was 18.9% at 650 nm, based on the data we collected. This is due to increased absorption in this area, which raises spectrum sensitivity and, eventually, quantum efficiency by generating more carriers in the depletion region.

CONCLUSION

The Q-Switched Nd-YAG pulsed laser has the ability to generate graphene and graphene oxide nanoparticles. The process of mixing chlorophyll with graphene and graphene oxide nanoparticles lead to an increase in the size of graphene nanoparticles because of aggregation and chlorophyll molecules may be interaction with graphene nanoparticles. The results reveal that modifying the surface morphology of the Si substrate to form SiNW successfully reduced the reflection loss of incident radiation over a broad spectral range. This remarkable property suggests that GNPs/Chl./SiNW nanocomposite are a good candidate for antireflective surfaces and absorption materials in photovoltaic cell. From Raman spectrum, the observed peak shifts and the emergence of additional peaks suggest that the size distribution of the silicon nanowires influences the spectral characteristics, underscoring the complex interactions between the components in the nanocomposite material. GNPs/Chl./SiNW nanocomposite was also used in the application of a detector with an efficiency of up to18.9% at 650 nm, based on the data we collected. This is due to increased absorption in this area, which raises spectrum sensitivity and, eventually, quantum efficiency by generating more carriers in the depletion region.

CONFLICT OF INTEREST

The authors declare that there is no conflict of interests regarding the publication of this manuscript.

REFERENCES

1. Huang Y, Duan X, Cui Y, Lauhon LJ, Kim K-H, Lieber CM. Logic Gates and Computation from Assembled Nanowire Building Blocks. Science. 2001;294(5545):1313-1317.
2. Cui Y, Lieber CM. Functional Nanoscale Electronic Devices Assembled Using Silicon Nanowire Building Blocks. Science. 2001;291(5505):851-853.
3. Cui Y, Duan X, Hu J, Lieber CM. Doping and Electrical Transport in Silicon Nanowires. The Journal of Physical Chemistry B. 2000;104(22):5213-5216.
4. Qu Y, Liao L, Li Y, Zhang H, Huang Y, Duan X. Electrically conductive and optically active porous silicon nanowires.

Nano Lett. 2009;9(12):4539-4543.
5. Huang R-G, Tham D, Wang D, Heath JR. High performance ring oscillators from 10-nm wide silicon nanowire field-effect transistors. Nano Research. 2011;4(10):1005-1012.
6. Wang D, Sheriff BA, McAlpine M, Heath JR. Development of ultra-high density silicon nanowire arrays for electronics applications. Nano Research. 2008;1(1):9-21.
7. Tang J, Wang H-T, Lee DH, Fardy M, Huo Z, Russell TP, et al. Holey Silicon as an Efficient Thermoelectric Material. Nano Lett. 2010;10(10):4279-4283.
8. Jeong S, Garnett EC, Wang S, Yu Z, Fan S, Brongersma ML, et al. Hybrid Silicon Nanocone–Polymer Solar Cells. Nano Lett. 2012;12(6):2971-2976.
9. Garnett E, Yang P. Light Trapping in Silicon Nanowire Solar Cells. Nano Lett. 2010;10(3):1082-1087.
10. Qu Y, Duan X. Progress, challenge and perspective of heterogeneous photocatalysts. Chem Soc Rev. 2013;42(7):2568-2580.
11. Thiyagu S, Devi BP, Pei Z. Fabrication of large area high density, ultra-low reflection silicon nanowire arrays for efficient solar cell applications. Nano Research. 2011;4(11):1136-1143.
12. Gunawardena J. Silicon dreams of cells into symbols. Nat Biotechnol. 2012;30(9):838-840.
13. Qing Q, Pal SK, Tian B, Duan X, Timko BP, Cohen-Karni T, et al. Nanowire transistor arrays for mapping neural circuits in acute brain slices. Proc Natl Acad Sci USA. 2010;107(5):1882-1887.
14. Wang G, Ling Y, Wang H, Xihong L, Li Y. Chemically modified nanostructures for photoelectrochemical water splitting. Journal of Photochemistry and Photobiology C: Photochemistry Reviews. 2014;19:35-51.
15. Wang G, Ling Y, Li Y. Oxygen-deficient metal oxide nanostructures for photoelectrochemical water oxidation and other applications. Nanoscale. 2012;4(21):6682.
16. Zhou H, Qu Y, Zeid T, Duan X. Towards highly efficient photocatalysts using semiconductor nanoarchitectures. Energy and Environmental Science. 2012;5(5):6732.
17. Qu Y, Zhong X, Li Y, Liao L, Huang Y, Duan X. Photocatalytic Properties of Porous Silicon Nanowires. J Mater Chem. 2010;20(18):3590-3594.
18. Wang P, Han L, Zhu C, Zhai Y, Dong S. Aqueous-phase synthesis of Ag-TiO2-reduced graphene oxide and Pt-TiO2-reduced graphene oxide hybrid nanostructures and their catalytic properties. Nano Research. 2011;4(11):1153-1162.
19. Bai J, Zhong X, Jiang S, Huang Y, Duan X. Graphene nanomesh. Nature nanotechnology. 2010;5(3):190-194.
20. Bai J, Cheng R, Xiu F, Liao L, Wang M, Shailos A, et al. Very large magnetoresistance in graphene nanoribbons. Nature nanotechnology. 2010;5(9):655-659.
21. Liao L, Lin Y-C, Bao M, Cheng R, Bai J, Liu Y, et al. High-speed graphene transistors with a self-aligned nanowire gate. Nature. 2010;467(7313):305-308.
22. Liao L, Bai J, Cheng R, Lin Y-C, Jiang S, Huang Y, et al. Top-gated graphene nanoribbon transistors with ultrathin high-k dielectrics. Nano Lett. 2010;10(5):1917-1921.
23. Liu Y, Cheng R, Liao L, Zhou H, Bai J, Liu G, et al. Plasmon resonance enhanced multicolour photodetection by graphene. Nature communications. 2011;2:579-579.
24. Wang G, Qian F, Saltikov CW, Jiao Y, Li Y. Microbial reduction of graphene oxide by Shewanella. Nano Research. 2011;4(6):563-570.
25. Wang B, Liddell KL, Wang J, Koger B, Keating CD, Zhu J. Oxide-on-graphene field effect bio-ready sensors. Nano Research. 2014;7(9):1263-1270.
26. Li X, Li J, Zhou X, Ma Y, Zheng Z, Duan X, et al. Silver nanoparticles protected by monolayer graphene as a stabilized substrate for surface enhanced Raman spectroscopy. Carbon. 2014;66:713-719.
27. Chen S, Brown L, Levendorf M, Cai W, Ju S-Y, Edgeworth J, et al. Oxidation Resistance of Graphene-Coated Cu and Cu/Ni Alloy. ACS Nano. 2011;5(2):1321-1327.
28. Xiang Q, Yu J. Graphene-Based Photocatalysts for Hydrogen Generation. The Journal of Physical Chemistry Letters. 2013;4(5):753-759.
29. Xiang Q, Yu J, Jaroniec M. Graphene-based semiconductor photocatalysts. Chem Soc Rev. 2012;41(2):782-796.
30. Wu H, Xu M, Da P, Li W, Jia D, Zheng G. WO_3–reduced graphene oxide composites with enhanced charge transfer for photoelectrochemical conversion. Physical Chemistry Chemical Physics. 2013;15(38):16138.
31. Bae S, Kim H, Lee Y, Xu X, Park J-S, Zheng Y, et al. Roll-to-roll production of 30-inch graphene films for transparent electrodes. Nature Nanotechnology. 2010;5(8):574-578.
32. Adhyaksa GWP, Prima EC, Lee DK, Ock I, Yatman S, Yuliarto B, et al. Nanoparticles: A Light Harvesting Antenna Using Natural Extract Graminoids Coupled with Plasmonic Metal Nanoparticles for Bio-Photovoltaic Cells (Adv. Energy Mater. 18/2014). Advanced Energy Materials. 2014;4(18).
33. Croce R, van Amerongen H. Natural strategies for photosynthetic light harvesting. Nat Chem Biol. 2014;10(7):492-501.
34. Otsuki J. Supramolecular approach towards light-harvesting materials based on porphyrins and chlorophylls. Journal of Materials Chemistry A. 2018;6(16):6710-6753.
35. Sommer Márquez AE, Lerner DA, Fetter G, Bosch P, Tichit D, Palomares E. Preparation of layered double hydroxide/chlorophyll a hybrid nano-antennae: a key step. Dalton Trans. 2014;43(27):10521-10528.
36. Gouterman M. Study of the Effects of Substitution on the Absorption Spectra of Porphin. The Journal of Chemical Physics. 1959;30(5):1139-1161.
37. Ceulemans A, Oldenhof W, Gorller-Walrand C, Vanquickenborne LG. Gouterman's "four-orbital" model and the MCD spectra of high-symmetry metalloporphyrins. Journal of the American Chemical Society. 1986;108(6):1155-1163.
38. Hug H, Bader M, Mair P, Glatzel T. Biophotovoltaics: Natural pigments in dye-sensitized solar cells. Applied Energy. 2014;115:216-225.
39. Wang L, Shi Y, Bai X, Xing Y, Zhang H, Wang L, et al. From marine plants to photovoltaic devices. Energy Environ Sci. 2014;7(1):343-346.
40. Wang X-F, Tamiaki H. Cyclic tetrapyrrole based molecules for dye-sensitized solar cells. Energy Environ Sci. 2010;3(1):94-106.
41. Chen S-Y, Lu Y-Y, Shih F-Y, Ho P-H, Chen Y-F, Chen C-W, et al. Biologically inspired graphene-chlorophyll phototransistors with high gain. Carbon. 2013;63:23-29.
42. Hecht DS, Ramirez RJA, Briman M, Artukovic E, Chichak KS, Stoddart JF, et al. Bioinspired Detection of Light Using a Porphyrin-Sensitized Single-Wall Nanotube Field Effect Transistor. Nano Lett. 2006;6(9):2031-2036.
43. Miyasaka T, Watanabe T, Fujishima A, Honda K. Highly efficient quantum conversion at chlorophyll a–lecithin mixed monolayer coated electrodes. Nature. 1979;277(5698):638-640.
44. Cai J, Wang J, Tian D, Huang J, Jiang L. Morphology-controlled self-assembled nanostructures of a porphyrin

derivative and their photoelectrochemical properties. RSC Adv. 2014;4(8):4063-4068.
45. Feng Y, Cheng H, Han J, Zheng X, Liu Y, Yang Y, et al. Chlorophyll sensitized $BiVO_4$ as photoanode for solar water splitting and CO_2 conversion. Chin Chem Lett. 2017;28(12):2254-2258.
46. Barazzouk S, Kamat PV, Hotchandani S. Photoinduced Electron Transfer between Chlorophyll a and Gold Nanoparticles. The Journal of Physical Chemistry B. 2004;109(2):716-723.
47. Kumari M, Sharma OP, Bagri RK, Nathawat BDS. Management of wilt disease of lentil through bio control agents and organic amendments in Rajasthan. Journal of Pharmacognosy and Phytochemistry. 2020;9(5):3248-3252.
48. Muhammad Asyraf Al-Wafiy L, Mohd Zaki Mohd Y, Suraya Ahmad K, Che Abdullah Che A, Mohd Firdaus M. Author response for "Green synthesis and characterisation of ZnO from citrus hystrix extracts for photocatalytic application". IOP Publishing; 2024.
49. Aziz C, Othman MA, Amer A, Ghanim AM, Swillam MA. Fabrication of crystalline silicon nanowires coated with graphene from graphene oxide on amorphous silicon substrate using excimer laser. Heliyon. 2024;10(13):e34023-e34023.
50. Bao X-Q, Fatima Cerqueira M, Alpuim P, Liu L. Silicon nanowire arrays coupled with cobalt phosphide spheres as low-cost photocathodes for efficient solar hydrogen evolution. Chem Commun. 2015;51(53):10742-10745.
51. Selvam M, Sakthipandi K, Suriyaprabha R, Saminathan K, Rajendran V. Synthesis and characterization of electrochemically-reduced graphene. Bull Mater Sci. 2013;36(7):1315-1321.
52. Gebreegziabher GG, Asemahegne AS, Ayele DW, Dhakshnamoorthy M, Kumar A. One-step synthesis and characterization of reduced graphene oxide using chemical exfoliation method. Materials Today Chemistry. 2019;12:233-239.
53. Huang Z, Geyer N, Werner P, de Boor J, Gösele U. Metal-Assisted Chemical Etching of Silicon: A Review. Adv Mater. 2010;23(2):285-308.
54. Luo X, Wang C, Luo S, Dong R, Tu X, Zeng G. Adsorption of As (III) and As (V) from water using magnetite Fe3O4-reduced graphite oxide–MnO2 nanocomposites. Chem Eng J. 2012;187:45-52.
55. Aziz HM, Al-Mamoori MHK, Aboud LH. Synthesis and Characterization of TiO_2-Rgo Nanocomposite by Pulsed Laser Ablation in Liquid (PLAL-Method). Journal of Physics: Conference Series. 2021;1818(1):012206.
56. Hassan EK. Structural and Optical Analysis of Rhodamine 6G Thin Films Prepared by Q-switched Nd: YAG Pulsed Laser Deposition. NeuroQuantology. 2020;18(3):45-50.
57. Al-Nafiey A, Al-Mamoori MHK, Alshrefi SM, shakir AK, Ahmed RT. One step to synthesis (rGO/Ni NPs) nanocomposite and using to adsorption dyes from aqueous solution. Materials Today: Proceedings. 2019;19:94-101.
58. Hutagalung SD, Fadhali MM, Areshi RA, Tan FD. Optical and Electrical Characteristics of Silicon Nanowires Prepared by Electroless Etching. Nanoscale research letters. 2017;12(1):425-425.
59. Ferrari AC, Meyer JC, Scardaci V, Casiraghi C, Lazzeri M, Mauri F, et al. Raman Spectrum of Graphene and Graphene Layers. Phys Rev Lett. 2006;97(18).
60. Gupta A, Chen G, Joshi P, Tadigadapa S, Eklund. Raman Scattering from High-Frequency Phonons in Supported n-Graphene Layer Films. Nano Lett. 2006;6(12):2667-2673.
61. Hiura H, Ebbesen TW, Tanigaki K, Takahashi H. Raman studies of carbon nanotubes. Chem Phys Lett. 1993;202(6):509-512.
62. Tan P, Deng Y, Zhao Q. Temperature-dependent Raman spectra and anomalous Raman phenomenon of highly oriented pyrolytic graphite. Physical Review B. 1998;58(9):5435-5439.
63. Pimenta MA, Dresselhaus G, Dresselhaus MS, Cançado LG, Jorio A, Saito R. Studying disorder in graphite-based systems by Raman spectroscopy. Phys Chem Chem Phys. 2007;9(11):1276-1290.
64. Basko DM, Piscanec S, Ferrari AC. Electron-electron interactions and doping dependence of the two-phonon Raman intensity in graphene. Physical Review B. 2009;80(16).
65. Wilkinson GR. R. J. H. Clark and R. E. Hester (Editors). Advances in infrared and Raman spectroscopy, vol. 12. Wiley, New York. 1985. Journal of Raman Spectroscopy. 1986;17(6):487-487.
66. Piscanec S, Ferrari AC, Cantoro M, Hofmann S, Zapien JA, Lifshitz Y, et al. Raman Spectrum of silicon nanowires. Materials Science and Engineering: C. 2003;23(6-8):931-934.
67. Li B, Yu D, Zhang S-L. Raman spectral study of silicon nanowires. Physical Review B. 1999;59(3):1645-1648.
68. Wang JN. An investigation of the deformation mechanism in grain size-sensitive Newtonian creep. Acta Mater. 2000;48(7):1517-1531.
69. Zhang S-L, Ding W, Yan Y, Qu J, Li B, Li L-y, et al. Variation of Raman feature on excitation wavelength in silicon nanowires. Appl Phys Lett. 2002;81(23):4446-4448.
70. Yu DP, Bai ZG, Ding Y, Hang QL, Zhang HZ, Wang JJ, et al. Nanoscale silicon wires synthesized using simple physical evaporation. Appl Phys Lett. 1998;72(26):3458-3460.
71. Hofmann S, Ducati C, Neill RJ, Piscanec S, Ferrari AC, Geng J, et al. Gold catalyzed growth of silicon nanowires by plasma enhanced chemical vapor deposition. J Appl Phys. 2003;94(9):6005-6012.
72. Gupta R, Xiong Q, Adu CK, Kim UJ, Eklund PC. Laser-Induced Fano Resonance Scattering in Silicon Nanowires. Nano Lett. 2003;3(5):627-631.
73. Habubi NF, Abd AN, Dawood MO, Reshak AH. Fabrication and Characterization of a p-AgO/PSi/n-Si Heterojunction for Solar Cell Applications. Silicon. 2016;10(2):371-376.